Chapter 2: Spatial Separation of Reaction Sites on Rutile TiO2 Nanorod by Exposing Crystal Faces and Development of Visible Light Responsive Rutile TiO2 Nanorod

Chapter One

Spatial separation of reaction sites on rutile TiO_2 nanorod by exposing crystal faces and development of visible light responsive rutile TiO_2 nanorod *

Teruhisa Ohno and Naoya Murakami
Department of Materials Science, Kyushu Institute of Technology, 1-1 Sensui-cho, Tobata Kitakyushu, Fukuoka 804-8550, Japan
tohno@che.kyutech.ac.jp

1.1 INTRODUCTION

TiO_2 has been intensively investigated or environmental remediation and energy conversion in the past several decades as a select platform on which an exceptionally wide range of appealing solid-state physical-chemical properties coexist with the potential for low cost and environmental remediation and energy technologies [1-3].

TiO_2 exists in three crystal structures: rutile, anatase and brookite. Each crystalline structure exhibits specific physical properties, band gap, surface states, etc. Rutile TiO_2 has some advantages over anatase such as higher chemical stability and higher refractive index. It is of fundamental significance to explore mild synthetic techniques by which particle shapes, nano- and micro-meter-scale morphologies, and crystallinity are well defined and controlled[3-5]. Moreover, surface chemistry of single crystalline rutile particles has been the subject of intensive studies because their chemical activity depends greatly on surface structures[6].

It has been reported that well-crystallized faceted particles showed enhanced photocatalytic activity compared to particles with poorly crystalline surfaces and that the photocatalytic activity increased with increase in crystallite size, the surface itself being an intrinsic defect[7].

Morphology, exposed crystal face-controlled synthesis of TiO_2 nanoparticles has long been paid attention in order to develop a high active TiO_2 photocatalyst. Among several kinds of synthetic methods for TiO_2 nanoparticles, a hydrothermal treatment has been drawing much attention for one of main synthetic techniques of TiO_2 nanocrystals because it directly produces well-crystallized nanocrystallities of a wide range of compositions of crystal phases under mild conditions. In addition, controlling exposed crystal faces of rutile nanorod TiO_2 by using surface morphology controlled reagents or chemical-etching reagents was also important strategy for further improvement their photocatalytic activities.

So many intensive efforts to improve the visible-light responsibility of TiO_2 photocatalyst involving impurity doping have been made in the last few decades [8-13].

However, impurity doping sometimes increase defects in TiO_2, which also work as recombination center and result in decrease of photocatalytic activity[14,15]. Recently, some visible-light responsive TiO_2 photocatalyst were developed by modification of metal surface complex which works as a sensitizer for a visible light[16-20]. This method has large advantages in simple preparation method and no introduction of defects in TiO_2. However, back electron transfer between

* Title footnote.

Book Title
First Author & Second Author

www.panstanford.com

injected electrons in TiO_2 bulk and oxidized metal ions on the surface of TiO_2 may easily proceeded resulting in significant decrease in a photocatalytic activity. Therefore, it is necessary for further improvement of photocatalytic activity under visible-light irradiation to modify metal ion site-selectively in the specific site on TiO_2 particles.

Our previous studies suggest that redox reaction proceed preferentially on specific exposed crystal faces of TiO_2[21-23]. This kind of preferential reaction was assigned by site-selective deposition of metal or metal oxide on the specific exposed crystal faces under photoexcitation[21-25].

As mentioned above, metal ion modification on TiO_2 for exhibiting visible light activity can be also applied to shape-controlled rutile TiO_2 nanorod for remarkable improvement of photocatalytic activity under visible light. In this case, crystal face-selective metal ion modification on shape-controlled particles with specific exposed crystal faces should be achieved, which results in remarkable suppression of back electron transfer in order to develop an ideal visible light responsive TiO_2 photocatalyst[26].

In this manuscript, a preparation of the morphology controlled rutile TiO_2 nanorod with exposed crystal faces by hydrothermal technique is summarized. The obtained rutile fine particles showed high levels of activity for degradation of organic compounds compared to the activity levels of anatase fine particles (ST-01) developed for environmental clean up by the company. In addition, exposition of a new high active crystal face of rutile TiO_2 nanorod is also demonstrated by using morphology controlled reagent or chemical etching reagents. After the treatments, remarkable photocatalytic activity improvement of the second step morphology controlled TiO_2 nanorod is observed compared to the original TiO_2 nanorod. Finally, the technology of visible light responsive treatment for morphology controlled rutile TiO_2 nanorod with exposed crystal faces by crystal face selective modification of metal ions on rutile TiO_2 nanorod is discussed. The metal ion modified rutile TiO_2 nanorod shows much higher activity than conventional visible light responsive N-doped TiO_2, which is commercially available in Japan.

1.2 MOROPHOLOGY CONTROLLED RUITLE TIO₂ NANOROD WITH EXPOSED CRYSTAL FACES

We carried out hydrothermal growth of rutile TiO_2 nanorod by using titanium trichloride ($TiCl_3$) with NaCl. Under our experimental conditions, rutile uniform TiO_2 nanorods were obtained, and developed crystal faces were observed. The obtained rutile TiO_2 nanorod showed high levels of activity for degradation of 2-propanol and acetaldehyde under UV irradiation compared to that of anatase fine particles (ST-01) developed for environmental clean up by the company in Japan. The surface chemistry of the rutile TiO_2 nanorod was also investigated. From photodeposition of Pt and PbO_2, we suggest that the (110) face provides reductive sites and that the (111) face provides oxidative sites. The results suggested that the crystal faces facilitate the separation of electrons and holes, resulting in improvement of photocatalytic activity.

1.2.1 *Experimental details for preparation and activity evaluation of rutile TiO_2 nanorod with exposed crystal faces*

In a typical synthesis procedure, a chemical solution was put in a sealed Teflon-lined autoclave reactor containing aqueous solution of titanium trichloride ($TiCl_3$) and sodium chloride (NaCl). The solutions were then put into a 200 °C oven. The substrate was centrifuged and rinsed with deionized water and then dried in a vacuum oven. Throughout this paper, samples are referred to as SH1 (NaCl 1 M), SH3 (NaCl 3 M) and SH5 (NaCl 5 M).

Photodeposition technique of Pt and PbO_2 was used for assignment of reduction and oxidation sites on exposed crystal faces of rutile TiO_2 nanorod, respectively.

For assignment of reduction site, rutile TiO_2 nanorod aqueous suspension (SH3) containing 2-propanol and hexachloroplatinic acid ($H_2PtCl_6{\cdot}6H_2O$) was irradiated with a mercury UV lamp. N_2 gas was purged through the suspension prior to UV irradiation in order to remove oxygen. After irradiation, the color of the powder changed from white to silver, and the suspension was centrifuged and washed with distilled water and then collected as powder (Pt loaded rutile TiO_2

nanorod) after drying at 70 °C under reduced pressure.

Photodeposition of PbO_2 as a result of oxidation of Pb^{2+} ions performed in order to assignment of oxidation site on exposed crystal face of Pt loaded rutile TiO_2 nanorod. This reaction was carried out in an aqueous Pt loaded rutile TiO_2 nanorod suspension containing $Pb(NO_3)_2$ under aerated conditions. The pH of the solution for this reaction was adjusted at 1.0 by the addition of nitric acid according to the literature[21-26]. After photoreaction using a 500 W Hg lamp, the color of the powder changed from silver to brown, indicating that PbO_2 had been deposited on the surface. Pt and PbO_2 particles deposited on rutile TiO_2 nanorod were observed in SEM, EDX and TEM images.

The photocatalytic activity of TiO_2 nanoparticles was evaluated by measuring the change in concentration of acetaldehyde and evolved CO_2 as a function of irradiation time. A Tedlar bag was used as the photoreactor vessel. TiO_2 powder was spread on the bottom of a glass dish, and this was placed in the reaction vessel. Five hundred ppmv of acetaldehyde was prepared in the vessel. The irradiation was conducted at room temperature after equilibrium between the gas and adsorbed acetaldehyde had been reached. The light source was a 500 W Xe-lamp. The light beam was passed through a UV-35 filter to cut off wavelength shorter than 350 nm. Fine stainless meshes were used as neutral density filters to adjust the irradiation intensity (10 or 30 mW cm^{-2}). After starting the irradiation, the decrease in acetaldehyde concentration and evolved carbon dioxide concentration was measured using a gas chromatograph. ST-01 having an anatase phase fine TiO_2 produced by Ishihara Sangyo CO. Ltd. was usually used as a reference catalyst.

1.2.2 *Results and discussion for rutile TiO_2 nanorod with exposed crystal faces*

XRD patterns of all the obtained particles were assigned to pure rutile phase and no other phases were detected. The intensity of diffraction peaks of the rutile TiO_2 nanorod becomes stronger with increase in NaCl concentration, indicating improvement in crystallinity of the rutile TiO_2 rod. The mean grain size was determined from Scherrer's equation. By applying Scherrer's formula to the rutile (110) diffraction peaks, the average crystallite sizes of the samples were found to be 66.0, 72.7 and 97.2 nm for samples SH1, SH3 and SH5, respectively.

Figure 1 shows TEM images and selected area electron diffraction (SAED) patterns taken from nanorods shown in TEM images. TEM images showed the rod-like shape with a triangular end and tetragonal rutile structure. TEM images (Figure 3a, 3c and 3e) showed that the shape of end of the rod changed from symmetric triangular tip to asymmetric triangular tip when the concentration of NaCl was increased. The SAED patterns of the exposed surface of the end of the rod and side surface of the rod are assigned to (111) and (110), respectively. The growth direction of the TiO_2 rod is the (001) direction. In addition, (001) crystal faces are exposed gradually with increase in NaCl concentration. A spot pattern indicates a single-crystalline nature of the rutile TiO_2 nanorods. From Figure 3, surface morphology of rutile TiO_2 is controlled with changing the concentration of NaCl.

Figure 2 shows photocatalytic evolution of CO_2 by

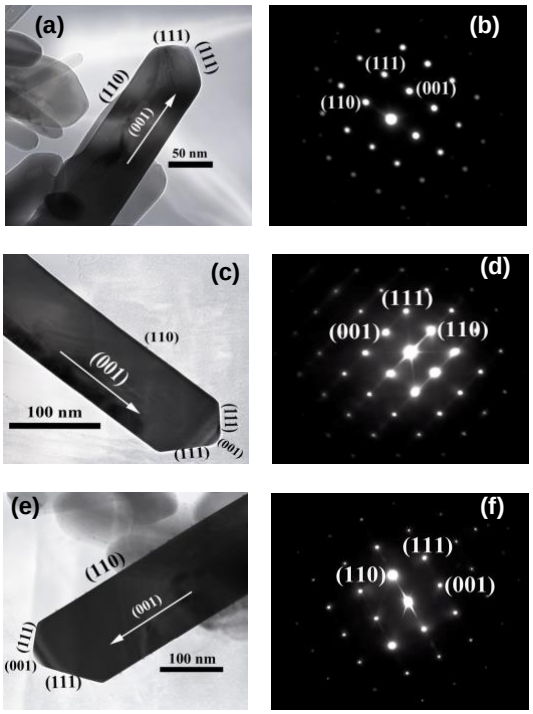

Figure 1. TEM images (a, c, e) and SAED patterns (b,

decomposition of acetaldehyde on reference TiO_2 and SH1, SH3 and SH5 at the light intensity of 10 mW cm^{-2}. Photocatalytic activity levels of rutile TiO_2 nanorods are higher than those of MT-600B and

ST-01. Among the rutile TiO_2 nanorods, SH5 showed the highest photocatalytic activity. The order of photocatalytic activities was SH5 > SH3 > ST-01 > SH1 > MT-600B as shown in Figure 2.

In order to clarify the origin of the remarkable photocatalytic activity improvement of rutile TiO_2

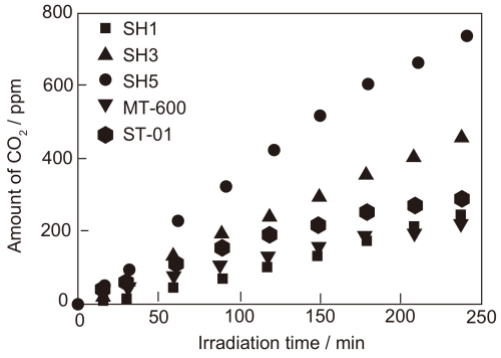

Figure 2. Time profiles of CO_2 evolution as a result of decomposition of acetaldehyde on TiO_2 at different concentrations of NaCl at light intensity 10 mW cm^{-2}. The experimental conditions were: $[acetaldehyde]_i$ = 500 ppm, $[TiO_2]$ = 10.4 mg/cm^2, UV light (λ > 350 nm) irradiated.

nanorods, it is important to identify the actual reactive sites on the surface of rutile TiO_2 nanorods.

It has been reported that oxidation and reduction sites on rutile maicro particles were exposed on the (011) and (110) faces, respectively[21]. Therefore,

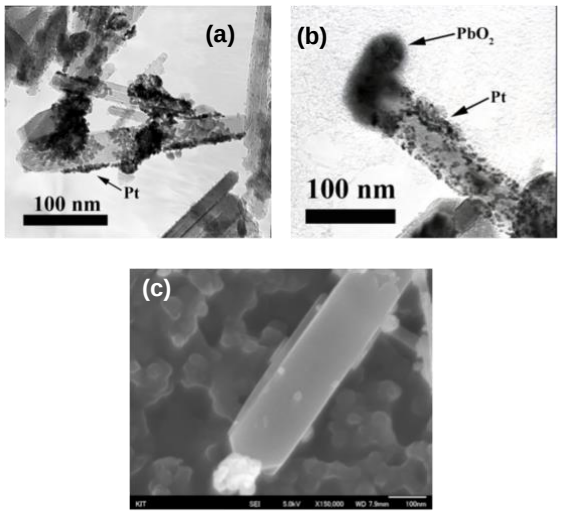

Figure 3. TEM image (a) of rutile TiO_2 nanorod (SH3) on which Pt particles were deposited. TEM image (b) and SEM image (c) of rutile TiO_2 nanorod (SH3) on which Pt and PbO_2 particles were deposited.

the exposing of well-developed faces on TiO_2 particles is advantageous for providing both oxidation and reduction sites which lead to remarkable suppression of back reactions on the surface of TiO_2 nanorod. Moreover, it is expected that the efficiency of electron-hole separation should be enhanced because of the difference in the electronic band structure between different crystals surfaces. Figure 3 shows TEM and SEM images of rutile TiO_2 nanorods showing rutile TiO_2 nanorods loaded with Pt (a) and PbO_2 (c), which were loaded on the Pt loaded rutile TiO_2 nanorod under UV irradiation. The deposited metals were analyzed by EDX (which is now shown here). Figure 3c shows SEM images of rutile TiO_2 particles showing PbO_2 deposits. Pt particles were deposited only on the (110) face as shown in Figure 3a. This result indicates that the reduction mainly proceeded on the (110) face of rutile TiO_2 nanorods. Figure 3b and 3c show that the PbO_2 particles were deposited on the (111) faces. This means that the (111) face provides the oxidation site for rutile TIO_2 nanorods. Our results suggest that the (110) face of rutile TiO_2 nanorods provides an effective reduction site and that the (111) face works as the oxidation site. Because of the spatially separation of reaction sites on TiO_2 nanorods such as reduction and oxidation sites are considered to be very efficient for some kinds of photocatalytic reactions.

Different surface energy levels of the conduction and valence bands are expected for different crystal faces of TiO_2 because of the atomic arrangements characteristic of these faces. The difference in the energy levels drives the electrons and holes to different crystal faces, leading to separation of electrons and holes[21]. The effective separation of oxidation and reduction sites of rutile particles, as shown in Figure 3, suggests that the electronic energy levels of the (110) face are lower than those of the (111) face[27]. Ohno et al. suggested that the isolation of oxidation or reduction site on the surface of TiO_2 particles is large enough to drive the photocatalytic oxidation of water on rutile particles when suitable electron acceptors are added to the solution[21]. The effective separation of oxidation and reduction sites on the surface of rutile TiO_2 particles should be important factor to obtain the high efficiency of some photocatalytic reactions.

As shown in Figure 2, an increase in particle size resulting from crystal growth did not cause a

decrease in photocatalytic activity, indicating that the photodegradation process is not surface-limited. However, control of rutile TiO_2 nanorods with exposed crystal surfaces is also one of important factor for improving photocatalytic activity of TiO_2. The large specific surface areas and small crystal sizes as well as high crystallinity of TiO_2 might usually play important roles in the enhancement of photocatalytic activities. However, spatial separation of reaction sites on the photocatalyst nanoparticle by controlling exposed crystal surface of the rutile TiO_2 nanorod is a more important factor for improvement of photocatalytic activity because a rutile TiO_2 nanorod having a small surface area (10-30 m^2g^{-1}) showed a higher level of photocatalytic activity than that of ST-01 with a large surface area (300 m^2g^{-1}).

1.3 NEWLY EXPOSDE CRYSTAL FACE OF RUITLE TIO_2 NANOROD BY USING CHEMICAL ETCHING TECHNIQUE

Rutile TiO_2 nanorods synthesized by hydrothermal treatment were etched by using of H_2O_2-NH_3 or H_2SO_4 solution as chemical etching reagents. New crystal faces were exposed on rutile TiO_2 nanorods by means of chemical etching treatment. In the case of H_2O_2-NH_3 solution treatment, the shape of the rutile TiO_2 nanorod changed to a sepal-like structure with reaction time. The dissolution of rutile TiO_2 nanorod mainly proceeded along [001]. When treated with sulfuric acid, the end [(111) face] of the rutile TiO_2 nanorod was gradually etched. The rutile TiO_2 nanorod finally exposed (001) and (021) faces during prolonged treatment time. In both cases, rutile TiO_2 nanorods were differently etched. The etched rutile TiO_2 nanorod showed higher photocatalytic activity for degradation of toluene in gas phase than the original particles.

1.3.1 *Experimental details for preparation and activity evaluation of chemically etched rutile TiO_2 nanorod*

The starting material for rutile TiO_2 nanorods was synthesized by using aqueous titanium trichloride with sodium chloride by means of hydrothermal treatment[22].

A synthesized rutile TiO_2 nanorod was added to the H_2O_2-NH_3 mixed solution and stirred for several hours at room temperature. After the treatment, the etched TiO_2 particles were separated by filtration, washed with water several times, and dried under aerated condition. For etching with sulfuric acid, prepared rutile TiO_2 nanorod was added to a flask containing concentrated sulfuric acid at room temperature and stirred for 6 h to 1 week. After the treatment, the etched TiO_2 particles were filtered and washed with 1% aqueous ammonia solution and then with deionized water.

Photocatalytic activity of rutile TiO_2 nanorods before and after etching treatment was evaluated by decrease in toluene in gas phase and evolved CO_2 as a result of photocatalytic mineralization of toluene. The evaluation procedure is as follows. TiO_2 powder was spread on a glass dish and the dish was placed in a reaction vessel with a volume of 125 cm^3 in the presence of 100 ppmv of toluene. A 500 W Xe-lamp was used as a light source. The light beam was passed through a UV-35 filter to cut off wavelengths shorter than 350 nm. Fine stainless meshes were used as neutral density filters to adjust the irradiation intensity (30 mW cm^{-2}). Irradiation was started at room temperature after a reaching equilibrium condition. After starting the irradiation, the evolved carbon dioxide and toluene were measured using a gas chromatograph equipped with a methanizer.

1.3.2 *Results and discussion for chemically etched rutile TiO_2 nanorod*

Rutile TiO_2 can be easily dissolved in H_2O_2-NH_3 mixed solution. Ohtani et al. reported that isolation of anantase TiO_2 was achieved by selective dissolution of rutile from P25 having a mixture of anatase and rutile phases[28]. Therefore, a small amount of NH_3 solution was used to prevent complete dissolution of rutile TiO_2 nanorods.

TiO_2 powder was suspended in H_2O_2-NH_3 mixed solution and stirred for several hours at room temperature, leading to dissolution of the solid to give a light-yellow sol which is a Ti^{4+}-H_2O_2 complex[28]. Figure 4 shows TEM and SEM images of a rutile TiO_2 nanorod with exposed crystal faces prepared according reference[22]. The assignment of crystal faces was reported previously[22].

SEM and TEM images of the rutile TiO_2 nanorod after treatment with H_2O_2-NH_3 mixed solution are shown in Figure 5. The rutile TiO_2 nanorod became

thinner with increase in etching time. As previously reported[22], **(a)** SAED patterns of the exposed surface of the rod end and side surfaces of the rutile TiO_2 rod were assigned to (111) and to (001) and (110), respectively (data not shown). The area of exposed (111) and (001) crystal faces gradually decreased with increase in reaction time. At the same time, a cone-shaped rod end was newly exposed and a crystal face assigned to the (110) face gradually decreased as shown in Figure 5. To assignment of the oxidation site, photodeposition of PbO_2 was carried out. PbO_2 was deposited on the oxidation site of TiO_2 by oxidation of Pb^{2+} ions dissolved in aqueous media[22, 29].

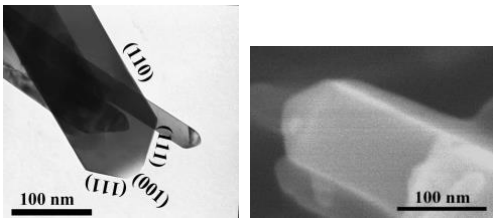

Figure 4. (a) TEM image and (b) SEM image of rutile particles present in the TiO_2 powder used in this study.

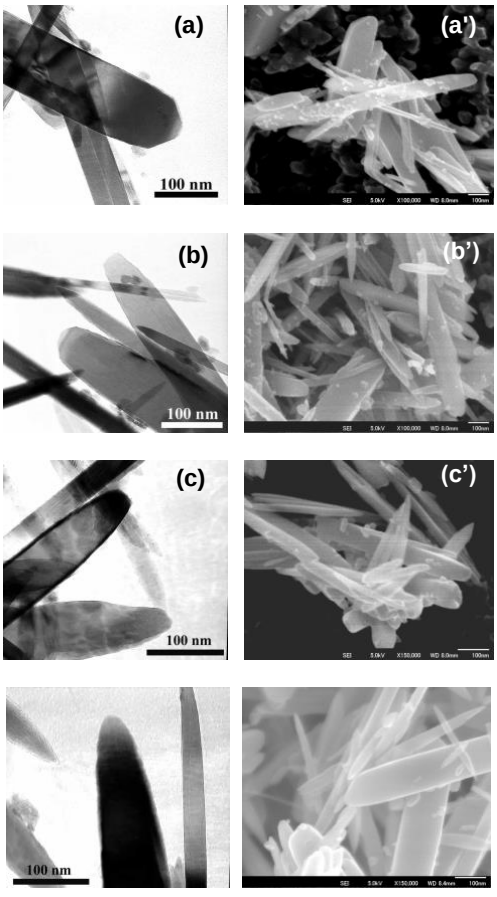

Figure 5. TEM images and SEM images of rutile particles after treatment with aqueous H_2O_2-NH_3 solution. The etching periods were about (a), (a'): 0.5

Figure 6 shows TEM and SEM images of chemically etched rutile TiO_2 nanorods

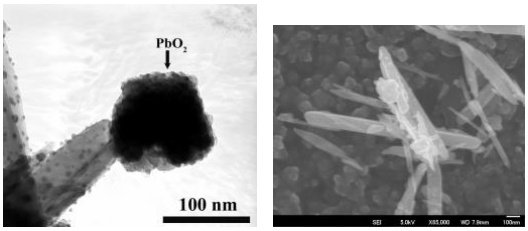

Figure 6. (a) TEM image and (b) SEM image of a rutile TiO_2 nanorod (H_2O_2-NH_3-1h) on which PbO_2 deposited with PbO_2 that were obtained after 1 h etching treatment. The deposited PbO_2 was analyzed by EDX (figure not shown). Figure 6 shows that the PbO_2 particles were deposited on the (111) and (001) faces on the rutile nanorod. The results indicate that the oxidation site on the rutile particles is on the exposed new cone-shaped rod end which agree with our previous studies[22, 29]. Therefore, the results suggest that effective isolation of oxidation sites of rutile TiO_2 nanorods is one of important factor for high reactivity.

Taguchi et al. reported that H_2SO_4 treatment at 200 °C generated new faces of rutile particles[30]. We tried this treatment for TiO_2 powder containing rutile TiO_2 nanorod. However, the color of rutile TiO_2 particles changed from white to pale gray and the shape of the particles became to deform at high temperatures (100 °C and 200 °C). The conditions for etching of rutile TiO_2 nanorods by sulfuric acid should be too severe to expose new crystal faces because particle size of our rutle TiO_2 nanorod is smaller than that reported in preiouspaper.29) Therefore, sulfuric acid treatment of the rutile TiO_2 nanorod had been carried out at room temperature. Figure 7 shows TEM and SEM images of rutile TiO_2 nanorod after sulfuric acid treatment for different time periods. TEM and SEM images before etching (Fig. 1) revealed that the shape of rod end of rutile TiO_2 was triangular-like tip. After sulfuric acid treatment, (001) face was exposed as a result of dissolution of (111) face as shown in Fig. 5. Generation of another new face was observed after treatment for one week. As seen in Figure 7e and 7e′, this new face is assigned to the (021) face which had been already assigned from previous paper[30]. As a result, (001) and (021) faces are generated at the tip of TiO_2 and, at the same time, the (111) face disappears from the rutile TiO_2 nanorod. However, no change in the (110) face of the rutile TiO_2 nanorod was detected after treatment.

Figure 8 shows

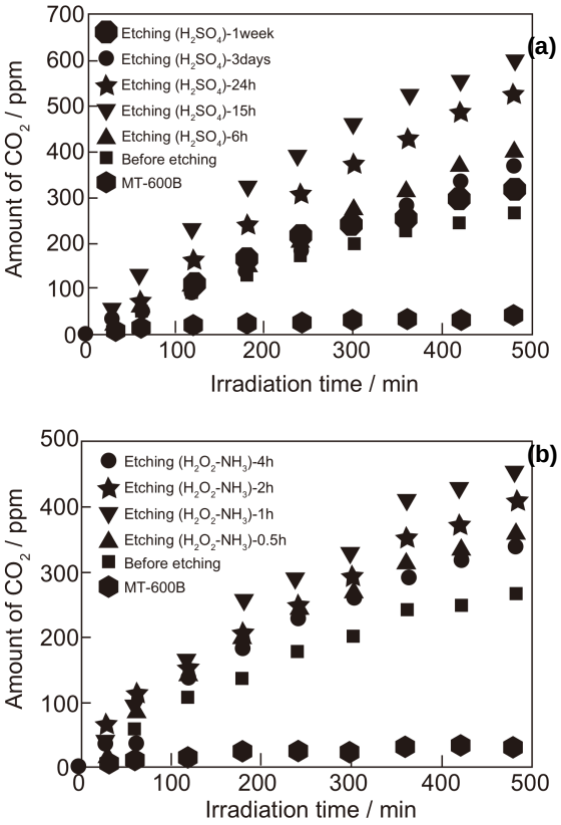

Figure 8. Time profiles of CO_2 evolution of toluene decomposition over TiO_2 particles prepared by treatment with (a) H_2O_2-NH_3 and (b) sulfuric acid at light intensity 30 mW cm^{-2}. The experimental

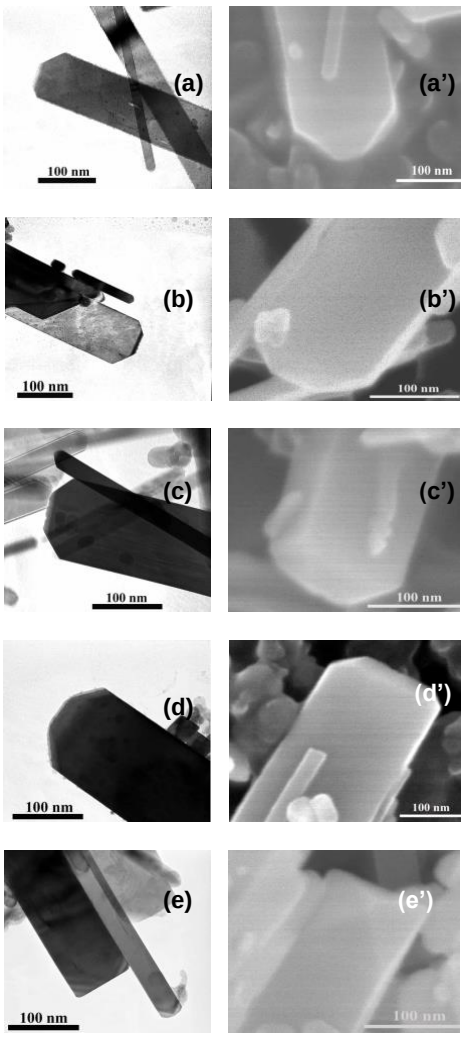

Figure 7. TEM images and SEM images of rutile particles after treatment with sulfuric acid. The etching periods were about (a), (a'): 6 h, (b), (b'): 15

photocatalytic activity of chemically etched rutile TiO_2 nanorod for evolution of CO_2 as a result of degradation of toluene at light intensity of 30 mW cm^{-2}.

Figure 8a shows the time course of CO_2 evolution over the rutile TiO_2 nanorods before and after treatment with H_2O_2-NH_3 solution. The photocatalytic activities of the etched rutile TiO_2 nanorod for toluene degradation were higher than those before etching, suggesting that etching is effective for improving the reaction. Rutile TiO_2 nanorod etched for 1 h with H_2O_2-NH_3 solution showed the highest photocatalytic activity among the treatments of rutile TiO_2 nanorods samples despite similar surface areas. These results suggest that the balance between oxidation and reduction

sites or newly exposed crystal faces is an important for high photocatalytic activity in the H_2O_2-NH_3 etching method. The rate-determining step of the reaction is thought to be not reduction of oxygen by photoecxited electrons but oxidation of toluene by holes generated photocatalytically because toluene is difficult to oxidize. Therefore, it is thought that photocatalytic activity of a rutile TiO_2 nanorod increases with increase in the oxidation sites on the rutile TiO_2 nanorod.

Figure 8b shows CO_2 evolution in degradation of toluene over rutile TiO_2 nanorods before and after treatment with an H_2SO_4 solution as a function of irradiation time. Commercially available MT-600B TiO_2 having rutile phase was also used as a reference for comparison. The etched rutile TiO_2 nanorods with a higher percentage of (001) faces showed higher photocatalytic performance. Therefore, the new exposed crystal face, (001), was thought to play an important role in improvement of photocatalytic activity of rutile TiO_2 nanorods. We previously reported that the exposed crystal face, (001), showed stronger oxidation power than that of the (111) crystal face[29].

1.4 VISIBLE LIGHT RESPONSIBE RUITLE TIO_2 NANOROD WITHOUT ETCHING TREATMENT MODIFIED SELECTIVELY WITH IRON(III) ION MODIFICATION OF EXPOSED CRYSTAL FACE

Trivalent iron(III) (Fe^{3+}) ions were site-selectively modified on {111} exposed crystal faces of rutile TiO_2 nanorod without etching treatment by utilizing adsorption property of iron(III)/iron(II) (Fe^{3+}/Fe^{2+}) ion on TiO_2 surface. The rutile TiO_2 nanorods with site-selective modification of Fe^{3+} ion showed a remarkable high photocatalytic activity under visible-light irradiation because separation of redox sites, i.e., oxidation and reduction proceed over Fe^{3+} ion modified on {111} faces and bare TiO_2 surface on {110} faces, respectively. Double-beam photoacoustic spectroscopic analyses suggest that the high activity of the TiO_2 with site-selective modification of Fe^{3+} ion is attributed to not only an efficient electron injection from Fe^{3+} ion but also an efficient reduction by injected electron on {110} faces.

1.4.1 *Experimental details for preparation and activity evaluation of Fe(III) modified rutile TiO_2 nanorod*

Non-site-selective modification of Fe^{3+} ion on the entire surface of rutile TiO_2 nanorod is as follows. An aqueous suspension composed of rutile TiO_2 nanorod and an aqueous solution of $Fe(NO_3)_3$ was stirred under an aerated condition. After filtration, the residue was washed with deionized water several times until the ionic conductivity of the supernatant was <10 $\mu S\ cm^{-2}$ in order to achieve complete removal of NO_3^- ion, and then the particles were dried under reduced pressure.

Preparation procedure of site-selective modification of Fe^{3+} ions on specific exposed faces is as follows. An aqueous suspension composed of rutile TiO_2 nanorod and an aqueous solution of $Fe(NO_3)_3$ with and without ethanol was stirred under an aerated condition. The stirring was carried out under UV irradiation with a 500-W super-high-pressure mercury lamp, the light intensity of which was 1.0 $mW\ cm^{-2}$. The supernatant and residue was separated by filtration immediately after the stirring. The residue was washed with deionized water several times until the ionic conductivity of the supernatant was <10 $\mu S\ cm^{-1}$, and then the particles were dried under reduced pressure.

Photocatalytic activities of samples were evaluated by photocatalytic decomposition over acetaldehyde. The glass dish contained 100 mg samples was placed in a 125 cm^3 Tedlar bag. Five hundred ppm of gaseous acetaldehyde was injected into the Tedlar bag, and photoirradiation was performed at room temperature after the acetaldehyde had reached adsorption equilibrium. The gaseous composition in the Tedlar bag was 79% of N_2, 21% of O_2, < 0.1 ppm of CO_2 and 500 ppm of acetaldehyde, and relative humidity was ca. 30%. A LED emitted light at a wavelength of ca. 455 nm (±15 nm) with an intensity of 1.0 $mW\ cm^{-2}$, was used for visible light irradiation. The concentrations of CH_3CHO and CO_2 were estimated by gas chromatography.

A gas-exchangeable photoacoustic (PA) cell equipped with two valves for gas flow was used, and a TiO_2 sample was placed in the cell. The atmosphere was controlled by a flow of nitrogen containing ethanol vapor (N_2 + EtOH) or artificial air containing ethanol vapor (air + EtOH), and the

measurements were conducted after shutting off the valves, i.e., in a closed system at room temperature. A LED emitting light at ca. 625 nm was used as a probe light, and the output intensity was modulated by a digital function generator at 80 Hz. In addition to the modulated light, a blue-LED (emitting light at ca. 470 nm, 8.1 mW cm^{-2}) was also used as simultaneous continuous irradiation for photoexcitation. The PA signal acquired by a condenser microphone buried in the cell was amplified and monitored by a digital lock-in amplifier. Detailed setups of double-beam photoacoustic (DB-PA) spectroscopic measurements have been reported previously[31].

1.4.2 *Results and discussion for visible light responsive rutile TiO_2 nanorod modified with Fe(III) ions*

The rutile TiO_2 nanorod without etching treatment have been prepared according to our previous paper[22,29]. The rutile TiO_2 nanorods used in this paper have exposed crystal faces with {110} and {111}. The specific surface area of the bare rutile rod was 34 m^2 g^{-1}.

Table 1 shows summary of Fe^{3+}-modified samples prepared by three kinds of Fe^{3+}-modification method. Valence state of iron ion on TiO_2 particles

Table 1. Fe^{3+}-modified TiO_2 prepared by different kinds of method and samples.

Name	Sample	Fe^{3+}(init) / wt%	Fe^{3+}(net) / wt%	preparation condition
D-004	rutile rod	0.04	0.04	dark
P-004	rutile rod	0.04	0.04	photo
D-01	rutile rod	0.10	0.10	dark
P-01	rutile rod	0.10	0.09	photo
PE-01	rutile rod	0.10	0.04	photo + EtOH
D-032	rutile rod	0.32	0.32	dark
P-032	rutile rod	0.32	0.22	photo
DMT	MT-600B	0.05	0.05	dark
PEMT	MT-600B	0.10	0.05	photo + EtOH

was confirmed to be trivalent state by XPS analyses. UV irradiation during Fe^{3+} modification decreased net amount of Fe^{3+} ion modified on the TiO_2 surface while almost of Fe^{3+} ion was adsorbed on the TiO_2 surface in dark. It is reported that Fe^{2+} ion hardly adsorb on TiO_2 surface compared to Fe^{3+} ion[32]. Therefore, Fe^{2+} ion produced as a result of reduction of Fe^{3+} ion by photoexcited electron in TiO_2 desorbed from TiO_2 surface into aqueous media. Addition of ethanol decreased net amount of modified Fe^{3+} ion because reduction of Fe^{3+} ion was accelerated due to an electron accumulation in TiO_2, which was induced by efficient hole consumption. Our previous study suggested that reduction and oxidation on the rutile TiO_2 nanorod proceed predominantly on {110} and {111} exposed crystal faces, respectively[22]. Therefore, Fe^{3+} ions mainly are expected to adsorb on {111} faces under UV irradiation because Fe^{3+} ion on {110} faces desorbs due to reduction of Fe^{3+} to Fe^{2+} (Scheme 1).

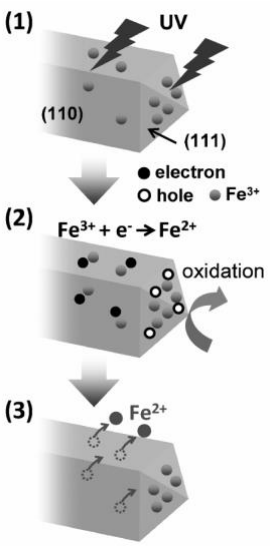

Scheme 1. Site selective modification on the shape controlled rutile rod with {110} and {111} exposed crystal faces.

Modification of Fe^{3+} ion induced color change form white to pale yellow as reported in previous study[19].

Figure 9 show UV-vis spectra of bare and Fe^{3+}-modified TiO_2. In the wavelength region between 400-500 nm of DR spectra, a red shift of photoabsorption edge was observed. Photoabsorption was increased with an increase in the net amount of Fe^{3+} ion adsorbed on the rutile TiO_2 nanorod.

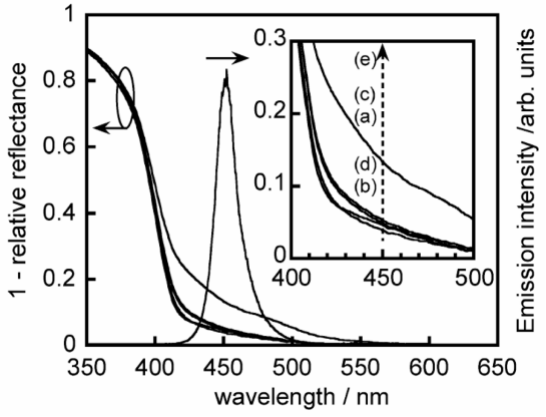

Figure 9. UV-vis spectra of (a) D-01, (b) P-01, (c) PE-01, (d) bare, and (e) D-032 and emission spectrum of LED used for photocatalytic evaluation.

Photocatalytic activity of Fe^{3+}-modified TiO_2 for decomposition of acetaldehyde was evaluated under visible light irradiation. Figure 10 shows CO_2 evolution as a result of acetaldehyde degradation as a function of photoirradiation time under visible-light irradiation. Photocatalytic activity of Fe^{3+}-modified TiO_2 was higher than bare TiO_2. This result indicates that Fe^{3+} ion modified on TiO_2 induce photocatalytic reaction under visible-light irradiation as follows[19];

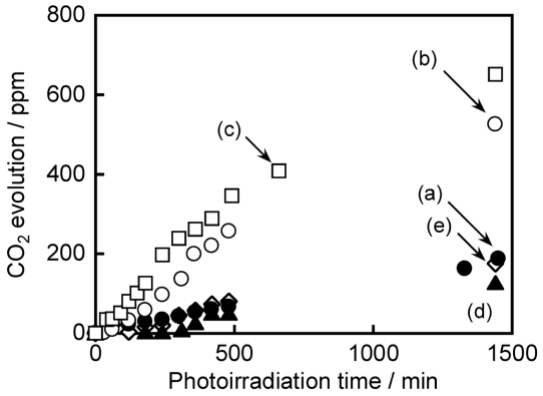

Figure 10. Time courses of CO_2 evolution for acetaldehyde decomposition over (a) D-01, (b) P-01, (c) PE-01, (d) bare TiO_2, and (e) N-TiO_2 under

(1) photoexcited Fe^{3+} ions injected electrons into TiO_2 and became an oxidized state of Fe^{3+} (Fe^{4+}), (2) injected electrons, which was trapped by Ti^{4+} in the bulk resulting in generation of Ti^{3+}, migrated to the surface of TiO_2 and reduced oxygen species on TiO_2 surface and (3) the oxidized state of Fe^{3+} ions (Fe^{4+}) oxidized acetaldehyde and go back to the initial state of metal ions (Fe^{3+}). PE-01 and P-01 showed higher photocatalytic activity than nitrogen-doped TiO_2 (N-TiO_2; Sumitomo Chemical Co.), which is well-known as a conventional visible-light responsive TiO_2. Moreover, photocatalytic activity of Fe^{3+}-modified TiO_2 showed dependence on its preparation method (PE-01 > P-01 > D-01). The plausible reason for difference of photocatalytic activity should be site selectivity of Fe^{3+} modification. In order to make clear it, following experiments were carried out.

Same modification method was applied to commercial rutile TiO_2, which has spherical shape without specific exposed crystal faces. Therefore, UV irradiation during Fe^{3+} modification is thought to induce no site-selective modification on the particle because redox reaction proceeds in the neighboring sites without being separated. Figure 11 shows CO_2 evolution for decomposition of

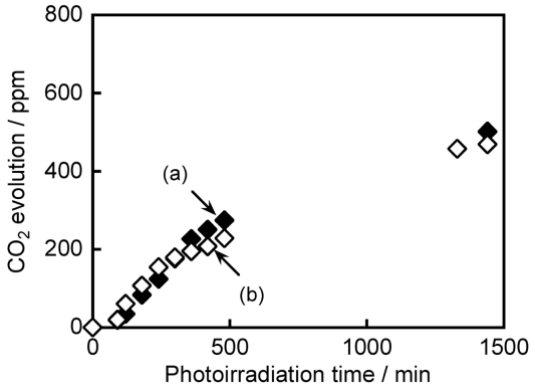

Figure 11. Time courses of CO_2 evolution for acetaldehyde decomposition over (a) DMT and (b) PEMT under visible-light irradiation.

acetaldehyde over Fe^{3+}-modified commercial rutile TiO_2 under visible-light irradiation as a function of irradiation time. These two samples were prepared by different kind of modification method, but same net amount of Fe^{3+} ion was modified between these samples by adjusting initial amount of Fe^{3+}. No difference of photocatalytic reaction was observed, regardless of the presence or absence of UV irradiation during Fe^{3+} modification. This indicates that the UV irradiation induced formation of same Fe^{3+} species for photocatalytic reaction as that prepared in dark. Therefore, the reason for high activity of P- and PE-samples is that UV irradiation during Fe^{3+} modification induces site-selective modification of Fe^{3+} ion. An excess amount of Fe^{3+} modification decreased photocatalytic activity even for P-samples because saturation limit of Fe^{3+} modification on {111} faces deteriorate site-selectively of Fe^{3+} modification, resulting in modification of Fe^{3+} ion on {110} faces. This indicates that modification on {110} faces decrease photocatalytic activity because an efficient reduction on {110} faces was retarded due to coverage of Fe^{3+} ion.

Behavior of injected electron in TiO_2 was observed by DB-PAS[31]. Figure 12 shows PA intensity for D-01, P-01, PE-01 and bare TiO_2 as a function of irradiation time under visible-light irradiation in the presence of N_2 + EtOH. PA intensity increased with visible-light irradiation because Ti^{4+} was reduced to Ti^{3+} by injected electrons from photoexcited Fe^{3+} ion. The saturation limit of PA intensity showed no

dependence on Fe^{3+}-modification method. This is reasonable result because photoabsorption of these samples was not so different from each other. This indicates that the plausible factor may

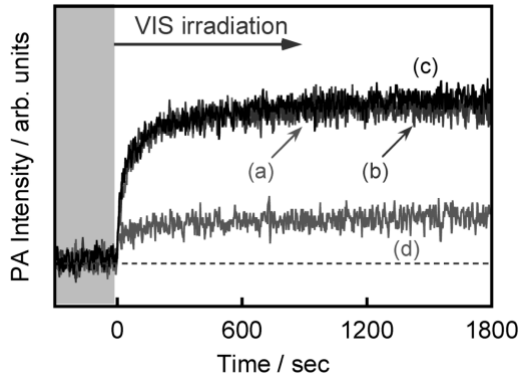

Figure 11. Time-course curves of PA signals of (a) D-01, (b) P-01, (c) PE-01, and (d) bare TiO_2 under visible-light irradiation in the presence of N_2 +

be efficiency of reduction on rutile TiO_2 nanorod modified with Fe^{3+} by injected electron.

DB-PA measurements in the presence of oxygen were also carried out in order to estimate efficiency of reduction by injected electron. Figure 12 shows time-course curve of PA intensity for D-01, P-01, PE-01 and bare TiO_2 under visible-light irradiation in the presence of air + EtOH. PA intensity attributed to Ti^{3+} formation was largely decreased because an electron accumulation was suppressed due to electron consumption by oxygen species on TiO_2 surface. Steady-state value of PA intensity showed dependence on modification method (D-01 > P-01 > PE-01). This suggests that reduction efficiently proceed on surface of P-01 and PE-01

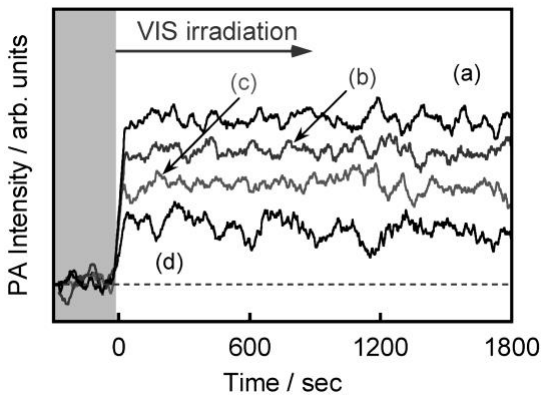

Figure 12. Time-course curves of PA signals with 50 points smoothing of (a) D-01, (b) P-01, (c) PE-01, and (d) bare TiO_2 under visible-light irradiation in

than that of D-01 because an efficient reduction of oxygen on {110} faces proceeded without retardation by site-selective coverage of Fe^{3+} ion on {111} face. The injected electron in the rutile TiO_2 nanorod site-selective modification of Fe_{3+} ions is thought to be prevented from being trapped by oxidized Fe^{3+} (Fe^{4+}) because the injected electrons should be efficiently consumed on {110} faces.

1.5 CONCLUSION

We have demonstrated that the morphotoly of rutile TiO_2 particles can be controlled by means of hydrothermal process and chemical etching treatment. The each exposed crystal surfaces of rutile nanorod shows the different activity such as oxidation and reduction, respectively resulting in improvement of charge separation. The photocatalytic activity of rutile TiO_2 nanorod shows higher activity than that of commercially available anatase TiO_2 fine particles in Japan.

The etched rutile TiO_2 nanorods showed higher photocatalytic activities than that of rutile TiO_2 nanorod without the etching treatment due to new exposed crystal faces. It was found that the photocatalytic activity depends on not surface area but surface structure of the TiO_2 nanorods, suggesting that electron-hole pair recombination plays an important role during the photodegradation of organic compounds.

UV irradiation during Fe^{3+}-modification on shape-controlled rutile TiO_2 nanorod showed high photocatalytic activity under visible-light irradiation because Fe^{3+} ion was site-selectively modified on {111} exposed crystal faces and redox reactions were spatially separated. DB-PA analyses indicate that photocatalytic activity was determined by not efficiency of electron injection but efficiency of reduction by injected electron. The efficiency of reduction was influenced by site-selectivity of Fe^{3+}-modification on {111} faces because Fe^{3+} ion on {110} faces retard an efficient reduction on bare TiO_2 surface.

References

1. Hoffmann, M. R., Martin, S. T., Choi, and W., Bahnemann, D. W. (1995) Environmental applications

of semiconductor photocatalysis, *Chem. Rev.*, **95,** pp. 69-96.
2. Choi, W. (2006) Pure and modified TiO2 photocatalysts and their environmental applications, *Catal. Surv. Asia*, **10**, pp. 16-28.
3. Chen, X. and Mao, S. S. (2007) Titanium dioxide nanomaterials: Synthesis, properties, modifications, and applications, *Chem. Rev.*, **107**, pp. 2891-2959.
4. Hosono, E., Fujihara, S., Kakiuchi, K. and Imai, H. (2004) Growth of submicrometer-scale rectangular parallelepiped rutile TiO_2 films in aqueous $TiCl_3$ solutions under hydrothermal conditions, *J. Am. Chem. Soc.,* **126**, pp. 7790-7791.
5. Neale, N. R. and Frank, A. J. (2007) Size and shape control of nanocrystallites in mesoporous TiO_2 films, *J. Mater. Chem.*, **17**, pp. 3216-3221.
6. Huang, X. and Pan, C. (2007) Large-scale synthesis of single-crystalline rutile TiO_2 nanorods via a one-step solution route *J. Cryst. Growth* **306,** 117-122.
7. Testino, A., Bellobono, I. R., Buscaglia, V., Canevali, C., D`Arienzo, M., Polizzi, S., Scotti, R., and Morazzoni, F. (2007) Optimizing the photocatalytic properties of hydrothermal TiO_2 by the control of phase composition and particle morphology. A systematic approach, *J. Am. Chem. Soc.,* **129**, pp. 3564-3575.
8. Sato, S. (1986) photocatalytic activity of nox-doped TiO_2 in the visible-light region, *Chem. Phys. Lett.* **123**, pp. 126-128.
9. Asahi, R., Morikawa, T., Ohwaki, T., Aoki, K. and Taga, Y. (2001) Visible-light photocatalysis in nitrogen-doped titanium oxides, *Science*, **293**, pp. 269-271.
10. Umebayashi, T., Yamaki, T., Itoh, H. and Asai, K. (2002) Band gap narrowing of titanium dioxide by sulfur doping, *Appl. Phys. Lett.*, **81**, pp. 454-456.
11. Ohno, T., Akiyoshi, M., Umebayashi, T., Asai, K., Mitsui, T. and Matsumura, M. (2004) Preparation of S-doped TiO_2 photocatalysts and their photocatalytic activities under visible light, *Appl. Catal. A: Gen.*, **265**, pp. 115-121.
12. Ohno, T., Tsubota, T., Nishijima, K. and Miyamoto, Z. (2004) Degradation of methylene blue on carbonate species-doped TiO_2 photocatalysts under visible light, *Chem. Lett.*, **33**, pp. 750-751.
13. Irie, H., Watanabe, Y. and Hashimoto, K. (2003) Carbon-doped anatase TiO_2 powders as a visible-light sensitive photocatalyst, *Chem. Lett.*, **32**, pp. 772-773.
14. Serpone, N. and Lawless, D. (1994) spectroscopic, photoconductivity, and photocatalytic studies of tio2 colloids - naked and with the lattice doped with Cr^{3+}, Fe^{3+}, and V^{5+} cations, *Langmuir*, **10**, pp. 643-652.
15. Ikeda, S., Sugiyama, N., Pal, B., Marci, G., Palmisano, L., Noguchi, H., Uosakid, K. and Ohtani, B. (2001) Photocatalytic activity of transition-metal-loaded titanium(IV) oxide powders suspended in aqueous solutions: Correlation with electron-hole recombination kinetics, *Phys. Chem. Chem. Phys.*, **3**, pp. 267-273.
16. Kisch, H., Zang, L., Lange, C., Maier, W. F., Antonius, C. and Meissner, D. (1998) Modified, amorphous titania - A hybrid semiconductor for detoxification and current generation by visible light, *Angew. Chem. Int. Ed.*, **37**, pp. 3034-3036.
17. Zang, L., Lange, C., Abraham, I., Storck, S., Maier, W. F. and Kisch, H. (1998) Amorphous microporous titania modified with platinum(IV) chloride - A new type of hybrid photocatalyst for visible light detoxification, *J. Phys. Chem. B*, **102**, pp. 10765-10771.
18. Zang, L., Macyk, W., Lange, C., Maier, W. F., Antonius, C., Meissner, D. and Kisch, H. (2000) Visible-light detoxification and charge generation by transition metal chloride modified titania, *Chem. Eur. J.*, **6**, pp. 379-384.
19. Macyk, W. and Kisch, H. (2001) Photosensitization of crystalline and amorphous titanium dioxide by platinum(IV) chloride surface complexes *Chem. Eur. J.*, **7**, pp. 1862-1867.
20. Murakami, N., Chiyoya, T., Tsubota, T. and Ohno, T. (2008) Switching redox site of photocatalytic reaction on titanium(IV) oxide particles modified with transition-metal ion controlled by irradiation wavelength, *Appl. Catal. A: Gen.*, **348**, 148-152.
21. Ohno, T., Sarukawa K. and Matsumura, M. (2002) Crystal faces of rutile and anatase TiO_2 particles and their roles in photocatalytic reactions, *New. J. Chem.*, **26**, 1167.
22. Bae, E., Murakami, N. and Ohno, T. (2009) Exposed crystal surface-controlled TiO_2 nanorods having rutile phase from $TiCl_3$ under hydrothermal conditions *J. Mol. Catal. A: Chem.*, **300**, pp. 72-79.
23. Murakami, N., Kurihara, Y., Tsubota, T. and Ohno, T. (2009) Shape-Controlled Anatase Titanium(IV) Oxide Particles Prepared by Hydrothermal Treatment of Peroxo Titanic Acid in the Presence of Polyvinyl Alcohol, *J. Phys. Chem. C,* **113**, pp. 3062-3069.
24. Kato, H., Asakura, K. and Kudo, A. (2003) Highly efficient water splitting into H_2 and O_2 over lanthanum-doped NaTaO3 photocatalysts with high crystallinity and surface nanostructure, *J. Am. Chem. Soc.*, **125**, 3082-3089.
25. Matsumoto, Y., Ida, S. and Inoue, T. (2008) Photodeposition of metal and metal oxide at the TiOx nanosheet to observe the photocatalytic active site, *J. Phys. Chem. C*, **112**, pp. 11614-11616.
26. Murakami, N., Ono, A., Nakamura, M., Tsubota, T. and Ohno, T. (2010) Development of a visible-light-responsive rutile rod by site-selective modification of iron(III) ion on {111} exposed crystal faces, *Appl Chem. A, General.,* **97**, pp. 115-119.

27. Oliver, P. M., Watson, G. W., Kelsey, E. T. and S Parker,. C. (1997) Atomistic simulation of the surface structure of the TiO_2 polymorphs rutile and anatase, *J. Mater. Chem.*, **7**, pp. 563-568.
28. Ohtani, B., Azuma, Y., Li, D., Ihara, T., and Abe, R. (2007) Isolation of anatase crystallites from anatase? Rutile mixed particles by sdissolution with hydrogen peroxide and ammonia, Trans. Mater. Res. Soc. Jpn., **32**, pp. 401-404.
29. Bae, E. and Ohno, T. (2009) Exposed crystal surface-controlled rutile TiO_2 nanorods prepared by hydrothermal treatment in the presence of poly(vinyl pyrrolidone)*Appl. Catal. B: Environ.*, **91**, pp. 634-639.
30. Taguchi, T., Saito, Y., Sarukawa, K., Ohno, T. and Matsumura, M. (2003) Formation of new crystal faces on TiO2 particles by treatment with aqueous HF solution or hot sulfuric acid, *New J. Chem.*, **27**, pp. 1304-1306.
31. Murakami, N., Mahaney, O. O. P., Abe, R., Torimoto, T. and Ohtani, B. (2007) Double-beam photoacoustic spectroscopic studies on transient absorption of Titanium(IV) oxide photocatalyst powdersj, *J. Phys. Chem. C,* **111**, pp. 11927-11935.
32. Ohno, T., Haga, D., Fujihara, K., Kaizaki, K. and Matsumura, M. (1997) Unique effects of iron(III) ions on photocatalytic and photoelectrochemical properties of titanium dioxide, *J. Phys. Chem. B*, **101**, pp. 6415-6419.